The initiation and evolution of transverse dunes: A literature review

Paul Jarvis

1 Introduction

2 Fluid flow

The first consideration when considering sedimentary processes is the driving flow. Although it is possible for sediment transport to occur in laminar flow (Charru and Mouilleron-Arnould, 2002; Charru et al., 2004; Mouilleron et al., 2009), the majority of research into the dynamics of ripples and dunes has considered turbulent conditions (Andreotti et al., 2002; Kroy et al., 2002; Langlois and Valance, 2007; Wierschem et al., 2008; Franklin and Charru, 2011; Charru and Franklin, 2012; Andreotti et al., 2012; Franklin, 2015), a reflection of the fact that these are relevant to the majority of natural systems. Therefore, we here summarise the fundamentals of turbulent flow, before discussing descriptions of wall bounded turbulent flow, both over flat and wavy surfaces.

2.1 Turbulence

The flow of any incompressible Newtonian fluid is described by the Navier-Stokes (NS) equation and the incompressibility relation:

$$\frac{\partial \boldsymbol{u}}{\partial t} + (\boldsymbol{u}\cdot\boldsymbol{\nabla})\boldsymbol{u} = -\frac{\boldsymbol{\nabla} p}{\rho} + \nu\nabla^2\boldsymbol{u}; \tag{1}$$

and

$$\boldsymbol{\nabla}\cdot\boldsymbol{u}. \tag{2}$$

These describe conservation of momentum and mass respectively where $\boldsymbol{u}(\boldsymbol{x},t)$ is the velocity field, $p(\boldsymbol{x},t)$ the pressure field, ρ the fluid density and ν the kinematic viscosity

of the fluid, whilst $\boldsymbol{x}$ and t are the spatial and temporal variables. If we define the components of the stress tensor $\boldsymbol{\tau}$ to be

$$\tau_{ij} = \rho\nu\left(\frac{\partial u_i}{\partial x_j} + \frac{\partial u_j}{\partial x_i}\right), \tag{3}$$

then the NS equation can be re-written as

$$\rho\left(\frac{\partial \boldsymbol{u}}{\partial t} + (\boldsymbol{u}\cdot\boldsymbol{\nabla})\boldsymbol{u}\right) = -\boldsymbol{\nabla}p + \boldsymbol{\nabla}\cdot\boldsymbol{\tau}. \tag{4}$$

It is useful to define the quantity vorticity, $\boldsymbol{\omega} = \boldsymbol{\nabla}\times\boldsymbol{u}$ which provides a measure of the local angular momentum of fluid elements. Vorticity is a useful quantity for a number of reasons. Firstly, it can be shown to obey a simpler equation than $\boldsymbol{u}$,

$$\frac{\partial \boldsymbol{\omega}}{\partial t} + (\boldsymbol{u}\cdot\boldsymbol{\nabla})\boldsymbol{\omega} = (\boldsymbol{\omega}\cdot\boldsymbol{\nabla})\boldsymbol{u} + \nu\nabla^2\boldsymbol{\omega}. \tag{5}$$

Secondly, it can be shown for two-dimensional flows that vorticity must be conserved within flow interiors; it cannot be created or destroyed but only advected or diffused. Vorticity can only be created at the boundaries of fluid domains, before being transferring into the interior. The origin of this creation is the strong velocity gradients within boundary layers.

The third use of vorticity is that is provides a starting point for a possible definition of turbulence. Turbulence is a poorly defined quantity. However, it is possible to picture turbulent eddies as regions of vorticity, with turbulence being an evolving field of eddies (Davidson, 2004). Here we will use the following definition of turbulence from Corrsin (1961), which has been modified by Davidson (2004): "Incompressible fluid turbulence is a spatially complex distribution of vorticity which advects intself in a chaotic manner in accordance with (5). The vorticity field is random in both space and time, and exhibits a wide and continuous distribution of length and time scales".

With a definition of turbulence, we can now proceed with a description of turbulent flow. This is achieved by decomposing $\boldsymbol{u}$, p and $\boldsymbol{\tau}$ into mean and fluctuation fields e.g. $\boldsymbol{u} = \bar{\boldsymbol{u}} + \boldsymbol{u'}$ where the bar denotes the mean field and the prime the fluctuation. The time-averaged NS equation is then shown to be given by

$$\rho\left(\frac{\partial \bar{u_i}}{\partial t} + \bar{u_j}\partial_j\bar{u_i}\right) = -\partial_i\bar{p} + \partial_i(\bar{\tau_{ij}} + \tau_{ij}^{\mathrm{R}}) \tag{6}$$

where the Reynolds stresses $\tau_{ij}^{\mathrm{R}} = -\rho\bar{u_i'u_j'}$. Additionally, time-averging the incompressibility relation yields both $\partial_i\bar{u_i} = 0$ and $\partial_i u_i' = 0$. Reynolds stresses are not stresses

in a physical sense. Physical stresses correspond to momentum fluxes between different fluid particles. Reynolds stresses correspond to momentum flux between the mean and fluctuation fields.

With this definition of Reynolds stresses, it is possible to manipulate the equations of motion to obtain an equation for them. This is algerbraically arduous and will not be repeated here but the end result contains a term $\partial_k(u_i' \bar{u_j'} u_k')$. The triple correlations here are unknown, but deriving an equation for them leads to a further set of unknowns $u_i' u_j' \bar{u_k'} u_l'$. The governing equations for these involves fifth-order correlations and so on. Hence, this statistical description of turbulence is undetermined - there are more unknowns than equations. This is called the closure problem. Numerous empirical models have been developed for a closure relation which completes the system of equations. The most widely used are eddy viscosity models, based on the principle that dissipation of momentum from the mean flow to the fluctuations by the Reynolds stresses is analogous to dissipation of momentum by viscous stresses. Hence, an analogous eddy viscosity ν_t can be defined as (Boussinesq, 1887)

$$\tau_{ij}^\mathrm{R} = \rho\nu_\mathrm{t}(\partial_j \bar{u_i} + \partial_i \bar{u_j}) - \frac{\rho \bar{u_k'} u_k' \delta_{ij}}{3}. \tag{7}$$

How ν_t is determined depends on the geometry of the flow. Since we are considering wall-bounded two-dimensional flows the most common method is to use Prandtl's mixing length model (Prandtl, 1925) (an analogue to the kinetic theory of viscosity) which gives

$$\nu_\mathrm{t} = l_\mathrm{m}^2 |\partial_z \bar{u_x}|, \tag{8}$$

where l_m is the mixing length which can be determined empirically. Whilst the model relies on dubious asumptions, it has been shown to be very succesful for one-dimensional shear flows.

2.2 Wall-bounded flow

We will initially consider turbulent flow over a flat, smooth, solid surface, with the mean flow directed in the x-direction, and the z-direction denoting the upward normal to the surface. The mean velocity in the interior of the flow (outside the boundary layer) is $\bar{\boldsymbol{u}} = (U_0, 0, 0)$ and the flow is unbounded as $z \to \infty$. The boundary layer thickness δ can be defined as the value of z at which $\bar{u_x}(z) = 0.99U_0$, although other measures exist (Pope, 2000). A significant amount of work has gone into studying the structure of this boundary layer. It has been postulated (Prandtl, 1925), and since verified both experimentally (Wei and Willmarth, 1989)and numerically (Kim et al., 1987), that there exists an inner layer close to the wall ($y/\delta \ll 1$) where $\bar{u}(x)$ depends on the viscous scales and is independent

of δ and U_0. The viscous lengthscale is defined as

$$\delta_\nu = \frac{\nu}{u_\tau}, \tag{9}$$

where u_τ is the friction velocity, defined as

$$u_\tau = \left(\frac{\tau_\mathrm{w}}{\rho}\right)^{1/2}, \tag{10}$$

and τ_w is the shear stress exerted on the wall. This postulate can be used to find the velocity profile within the inner layer. Defining $y^+ = y/\delta_\nu$, it can be shown that for small y^+ there exists a viscous sublayer where (Pope, 2000)

$$\bar{u}_x(z) = \frac{u_\tau z}{\delta_\nu}, \tag{11}$$

and for $y^+ \gg 1$, there is a so called log-law region (von Kármán, 1930) where

$$\bar{u}_x(z) = \frac{u_\tau}{\kappa} \ln\left(\frac{z}{z_0}\right). \tag{12}$$

Here κ is the von Kármán constant and z is a constant of integration called the hydrodynamical roughness, found by matching to the profile in the viscous sublayer. Experimental and numerical studies have shown that the viscous sublayer typically extends to $y^+ < 5$ and the log-law region for $y^+ > 30$, $y/\delta < 0.3$ (Kim et al., 1987; Wei and Willmarth, 1989), with $\kappa \approx 0.4$. The transition between these two parts of the inner layer is called the buffer layer. Beyond the inner layer, there exists an outer layer, which has predominantly been described empirically (Pope, 2000).

The mixing length for wall-bounded flow is given by (Pope, 2000)

$$l_\mathrm{m} = \kappa z \left[1 - \exp\left(\frac{z}{\alpha\delta_\nu}\right)\right], \tag{13}$$

where $\alpha \approx 25$ is the van Driest number.

For a rough surface, the roughness can be described by a bed of grains of characteristic diameter d fixed at $z = 0$ (Charru et al., 2013). For $d/\delta_\nu \lesssim 5$ the effect of the roughness in the log-law region is negligible, as the disturbance to the flow is contained within the viscous sublayer. However, at larger d, the flow is said to be hydrodynamically rough, and experimental observations are used to estimate the hydrodynamic roughness (Bagnold, 1941; Kamphuis, 1974). Various works use $l_m = \kappa(z + z_0)$ as the mixing length for a hydrodynamically rough flow (Fourrière et al., 2010).

2.3 Flow over a perturbed profile

We now consider the flow over a sinusoidal profile $\zeta = \zeta_0 \cos(kx)$, where ζ_0 is the amplitude of the perturbations to the surface, and k is the wavenumber. If the gradient of the profile is small ($k\zeta_0 \ll 1$), then the resultant perturbation to the flow will be linear. For example, the resultant perturbation to the shear-stress in the x-direction at the fluid surface can be expressed as (Kroy et al., 2002; Charru et al., 2013)

$$\tau_\mathrm{b} = \frac{\hat{\tau} e^{ikx} + \hat{\tau}^* e^{-ikx}}{2}, \quad \text{where} \quad \hat{\tau} = \tau_\mathrm{w}(A + iB)k\zeta_0. \tag{14}$$

The periodic functional form of τ_b is due to the periodic nature of the solid boundary. The contribution from A is in-phase with the surface disturbance and that from B is in quadrature.

Depending on the relative values of the different length scales in the problem (k^{-1}, δ_ν), the perturbation to the flow occurs in different hydrodynamic regimes. For the case that the flow disturbance is confined to the viscous sublayer ($k\delta_\nu ll 1$), the flow disturbance due to the surface perturbations is laminar, and has a two-layered structure (Charru et al., 2013): an inner viscous layer, and an outer inertial layer. Remember, both of these layers are within the viscous sublayer and are different from the much larger inner and outer layers that describe the coarser structure of the general boundary layer. The shear-stress on the solid surface can be evaluated, and both A and B in equation (14) are found to both be positive. This means the maximum of the shear stress is always located upstream of the crests (Benjamin, 1958; Charru and Hinch, 2000; Charru et al., 2013).

The other possibility is that the flow disturbance extends beyond the viscous sublayer ($k\delta_\nu > 1$). It can again be shown that the flow disturbance has a multi-layered structure, but here the perturbation is turbulent. Jackson and Hunt (1975) and Sykes (1980) considered two-layers: a thin, turbulent layer outside the viscous sublayer dominated by gradients in Reynolds stresses, overlain by an inertia-dominated layer that continued up to the outer layer of the boundary layer. This description was later improved wth the inclusion of a middle layer which improved matching (Hunt et al., 1988; Belcher and Hunt, 1998). As for small peaks, the maximum shear stress is again found upstream of the crests (Hunt et al., 1988; Belcher and Hunt, 1998; Kroy et al., 2002; Charru et al., 2013).

As well as the laminar and turbulent regime, there is a transitional regime where neither viscous effects nor turbulent fluctuations can be ignored. Thus far, only empirically verified simple parameterisations of the viscous sublayer thickness have been used in describing this regime (Abrams and Hanratty, 1985; Frederick and Hanratty, 1988), and a true physical understanding of the behaviour is lacking.

2.3.1 Other flow features

Clearly, the above description of the effect of shallow, sinusoidal disturbances to the wall doesn't completely describe flow regimes for natural bedforms. Perhaps the most obvious difference involves the shape of the obstacle. The typical, two-dimensional dune shape is asymmetric, with a long upstream (stoss) side and a shorter downstream (lee) side. The reasons for this shape will be discussed below but it is clear that any model of flow over bedforms must account for this. Numerical investigations have studied the response of flow to obstacles of different shapes (Richards and Taylor, 1981; Yue et al., 2006) and, as long as obstacle slopes are small, linear descriptions of flow response are still valid.

As slopes become steeper ($k\zeta_0 \approx 0.1$), non-linear effects become important. To account for these it is neccessary to generalise equation (14) to include higher order terms in the expansion,

$$\tau_\mathrm{b} = \frac{1}{2}\sum_{n=1}^{N}(\hat{\tau_n}e^{ikx} + \hat{\tau_n}^* e^{-ikx})^n, \quad \text{where} \quad \hat{\tau_n} = \tau_0(A_n + iB_n)(k\zeta_0). \tag{15}$$

This reduces to equation (14) for the case $N = 1$. Some weakly non-linear analysis have been performed, using a small number of terms to evaluate the perturbation to the flow field (Caponi et al., 1982; Andreotti et al., 2009), and these successfully predict changes to the velocity profile and surface shear stress for $k\zeta_0 \lesssim 0.3$ (Kuzan et al., 1989). Of particular interest is the deviation to the shear stress profile as higher harmonics become significant (Zilker et al., 1977; Richards and Taylor, 1981).

Further increasing $k\zeta_0$ leads to the occurence of a strongly nonlinear feature called flow separation. This occurs as the flow passes over the crest of an obstacle, and slows down as the flow depth increases. If the extent of slowing down in the fluid adjacent to the surface is much greater than in the overlying fluid, this can lead to the formation of a recicrulation bubble behind the obstacle (figure 1). The streamlines separate from the surface at the point S and reattach at R.

Recirculation bubbles have been observed in numerous experimental and numerical studies of flow over wavy boundaries, with focus on the conditions that lead to flow separation (Zilker and Hanratty, 1979; Richards and Taylor, 1981; Kuzan et al., 1989), the location, size and shape of the recirculation bubble (Buckles et al., 1984), and the effect of the bubble of the surface shear stress (Finnigan et al., 1990; Henn and Sykes, 1999). It is also important to note that for turbulent flows, the turbulent fluctuations mean that, although the mean flow may be steady, the instantaneous flow varies, meaning the positions of the separation and reattachment points may change with time (Zilker and Hanratty, 1979). This presents a challenge when defining the extent of the recirculation bubble for turbulent flows. To handle this, the intermittency $\gamma(x, z)$ is defined as the fraction of the time that the flow is directed in the positive x direction (Simpson et al., 1981). Contours of intermittancy can then be used to define the region of reverse flow and the recirculation bubbles (Buckles et al., 1984).

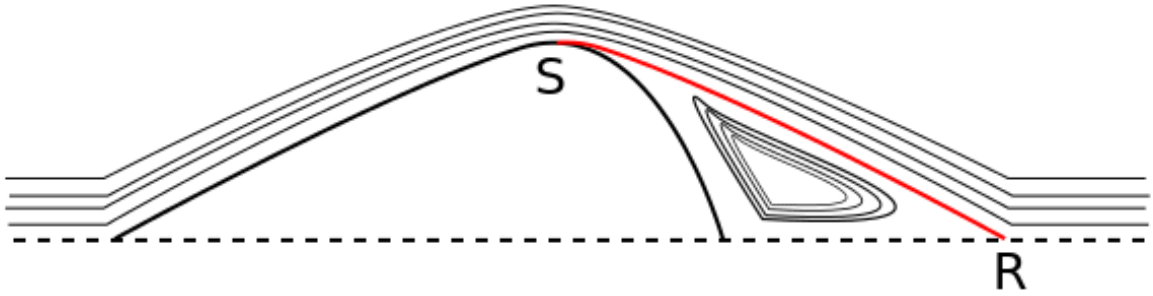

Figure 1: Schematic showing flow separation behind an obstacle. Streamlines separate from the solid surface at point S and rejoin at R, forming a recirculation zone bounded by the solid surface and the red curve (called the separation streamline).

At the separation point, a layer of high vorticity is ejected from the boundary into the interior of the flow (Yue et al., 2006). If the wavelength of the obstacles is shorter than the distance over which this vorticity disperses, then vertical velocity profiles in the flow can become highly chaotic and far removed from the simple analytical descriptions of wall flow.

3 Types of sedimentary bedforms

There are a variety of different types of sedimentary bedforms found in nature, with the diversity reflecting the hugely variable conditions under which erosion and sedimentation processes occur. Most generally, there are two types of environment in which bedforms can be found: subaerial; and subaqueous. Subaerial bedforms result from the flow of air over a granular medium, such as a desert, beach, snow depsoti or volcanic ash deposit. Subaqueous bedforms are created by the action of water, and can be found on river-beds, shallow coastel regions, or deeper continental shelves. Within this hierarchy, further variability in shape and size of bedform originates from spatial and temporal variations in flow-speed, flow-depth, particle size, particle density and local topography. Examples of different types of bedforms are shown in figure 2.

The diverse range of environments and conditions in which bedforms exist, and the extensive variability in their morphologies means their classification has historically been inconsistent (Ashley, 1990). The term ‘ripple’ has typically been used to describe small structures of O(1cm) with ‘dunes’ used for larger deposits $> O$(10cm) (Julien, 1995). However, these terms have often been used interhcangably in the literature. In an attempt to develop a formal classification, it has been noted that size distributions of both subaerial and subaqueous bedforms contain two distinct populations with different modes (Lancaster, 1988; Ashley, 1990), with the smaller group assigned as ripples, and the

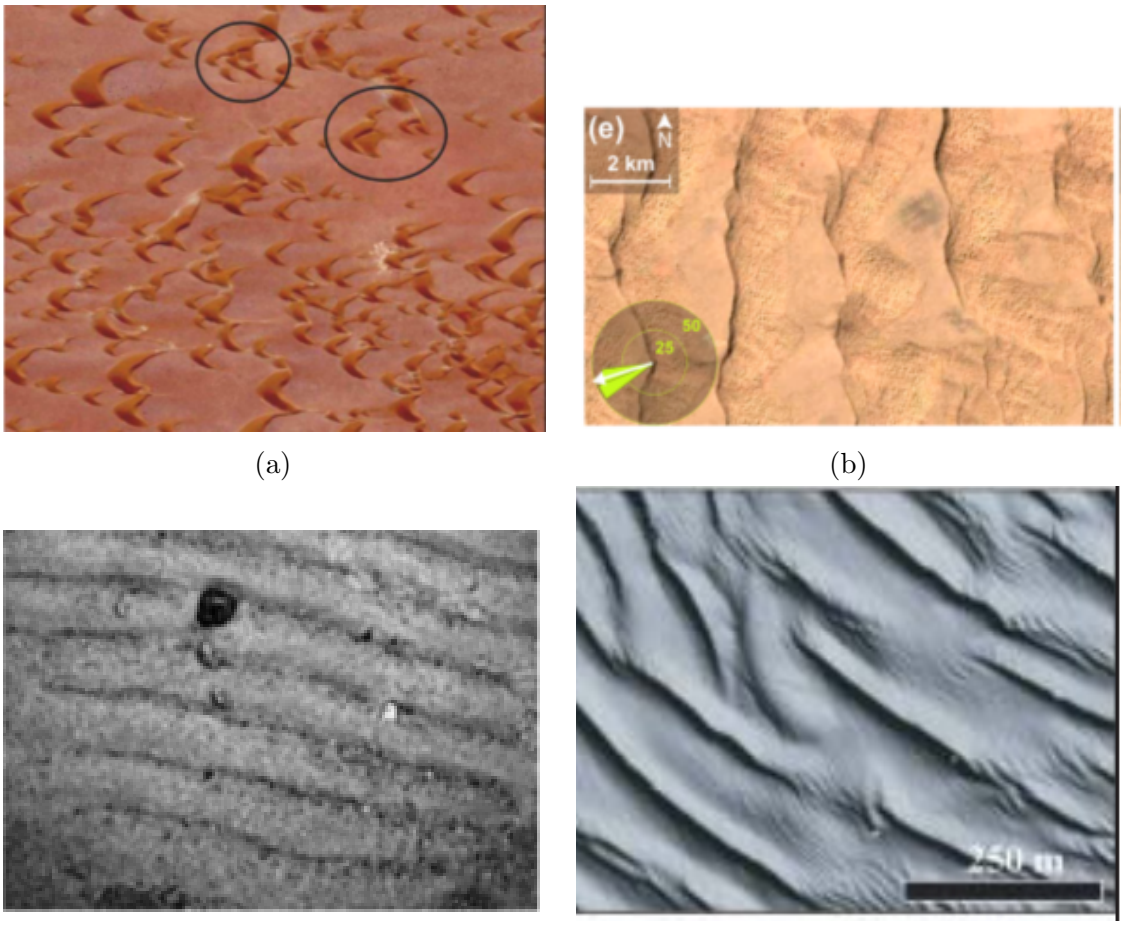

(a) (b)

(c) (d)

Figure 2: Examples of bedforms. a) A field of barchan dunes from Morocco. (Durán et al., 2011). b) Transverse dune field in the East Taklamakan desert, China (Gao et al., 2015). Subaqueous ripples in Zion National Park, USA (Andreotti et al., 2012). d) Large subaqueous dunes in San Francisco Bay, USA (Barnard et al., 2006).

larger as dunes. This is a phenomenological classification founded in field observations. Andreotti et al. (2012) used a mechanistic classification; ripples were defined as having a wavelength much smaller than the flow depth, and formed from an instability of the sediment surface. Dunes had a wavelength comparable to the flow depth, and formed from the merging of dunes, a process called pattern coarsening. Whether these definitions are equivalent remains unknown, but since we are here investigating bedforms from a mechanistic viewpoint, we will use the definition of Andreotti et al. (2012).

The dunes and ripples considered here will all be transverse. Flow is directed in the x-direction and the bed geometry can be completely described by a curve in a vertical plane.

4 Modes of sediment transport

In order for a flow to transport any sediment, it is neccessary for the for the shear stress exerted on the bed surface to be sufficient to lift a particle up and over its neighbours. Hence, the lift force provided by the flow must be sufficient to overcome gravity. This balance is quantified through the Shields number

$$\Theta = \frac{\tau}{(\rho_\mathrm{p} - \rho_\mathrm{f})gd}, \tag{16}$$

where τ is the surface shear stress, ρ_p and ρ_f are the densities of the particles and fluid respectively, $g = 9.81$ m s^{-2} is the acceleration due to gravity and d is the particle diameter. Hence, there is some critical value of the Shields number at which motion becomes possible.

Broadly, there are three mechanisms describing how sediment can be transported by an overlying fluid (Bagnold, 1941). For Shields numbers just above the threshold for motion, bedload transport (reptation, creep) will occur, whereby particles slide and roll across the surface. With increasing flow velocity, these particles can be lifted higher into the flow, and 'hop' across the bed following ballistic trajectores, a process called saltation. Once the size of turbulent fluctuations in the vertical fluid velocity are comparable to the settling velocity of the particles, they can become suspended in the fluid and are transported as suspended load. Each of these processes has been studied and we'll briefly review them here.

Bedload transport can be modelled as a layer of mobile grains at the sediment surface. For viscous flow, this can be modelled as viscous resuspension (Leighton and Acrivos, 1986), whereby the shear imposed on the bed by the flow initiates diffusion of particles upwards (Leighton and Acrivos, 1987). Using this model, it is possible to derive a theoretical law for the particle flux that depends on the Shields number, and a correction due to the effect of gravity on a slope (Charru and Mouilleron-Arnould, 2002) (see table 1). Bedload transport has been experimentally studied in an annular flume and a process

Table 1: Summary of sediment transport models.

Type of transport	Flow regime	Transport Law	Reference
Bed-load	Viscous	$q \sim (\Theta - \Theta_c)^2(\hat{\theta} - \hat{\theta_c})$	(Charru and Mouilleron-Arnould, 2002)
Bed-load	Viscous	$q \sim \Theta(\Theta - \Theta_c)$	(Charru et al., 2004)

called armouring has been observed (Charru et al., 2004). During this phenomenon, transported particles settle into gaps between stationary particles, increasing the packing fraction of the bed. This leads to a reduction in height of the bed and an increase in Θ_c. The same experimentaly study also determined an empirical transport law different to that previously determined.

An alternative model for bedload transport involves finding explicit expressions for erosion and deposition rates (Charru and Hinch, 2006). Use of this model shows that there exists length- and time-scales over which the sediment flux responds to changes in bed topography or flow conditions. An important feature of all sediment transporting flows is that there is a finite limit to the amount of sediment that can be transported by a given flow, quantified through the saturated sediment flux q_{sat} (Bagnold, 1941; Owen, 1964). The physical origin for this saturation can be explained by realising that there is a negative feedback between the flow and entrainment. An increase in the flow velocity (and therefore bed shear stress) will increase entrainment, but the entrained grains themselves exert a resistive stress on the flow. This leads to a steady state where the rates of erosion and deposition balance each other (Andreotti and Claudin, 2013). The erosion-deposition model can be used to derive an expression descibing the behaviour of transient states displaced from this saturated state

$$T_{\text{sat}}\frac{\partial q(x,t)}{\partial t} + L_{\text{sat}}\frac{\partial q(x,t)}{\partial x} = q_{\text{sat}} - q(x,t). \tag{17}$$

where T_{sat} is the saturation time and L_{sat} is the saturation length. Typically, the timescale of sediment transport is much shorter than changes to flow or bed topography, so the first term is typically neglected. The erosion-deposition model suggests that for bed-load transport in a viscous flow $L_{\text{sat}} \sim \rho_p d/\rho_f$ (Charru, 2006).

Since the timescale of sediment transport is much shorter than bed evolution, the first term can typically be neglected. As mentioned above, the expression for L_{sat} depends on the mechanism of transport (Andreotti et al., 2012). For suspended transport, the length corresponds to the distance a particle will travel before settling out, $L_{\text{sat}} \propto UH/V_{\text{fall}}$, where U is the mean flow velocity, V_{fall} is the settling velocity of the particle and H is the depth of the flow (Claudin et al., 2011). A similar principle can be used to determine the saturation length for bedload transport. Assuming the transport takes place within a layer of lengthscale d, the $L_{\text{sat}} \propto Ud/V_{\text{fall}}$ (Charru, 2006). For saltation, the lengthscale

can be considered as the length needed for a particle to reach its equilibrium velocity (Andreotti et al., 2002), for which it can be shown $L_{\mathrm{sat}} \propto \rho_{\mathrm{p}} d/\rho_{\mathrm{f}}$. Despite the different transport mechanisms having different saturation lengths, L_{sat} enters into the dynamics identically for all three cases, allowing the same methods to be used to study bedforms regardless of the transport mechanism.

5 Initiation of transverse structures

6 Coarsening

7 Open questions

References

J. Abrams and T. J. Hanratty. Relaxation effects observed for turbulent flow over a wavy surface. *J. Fluid Mech.*, 151:443–455, 1985.

B. Andreotti and P. Claudin. Aeolian and subaqeuous bedforms in shear flows. *Phil. Trans. R. Soc. A*, 371, 2013.

B. Andreotti, P. Claudin, and S. Douady. Selection of dune shapes and velocities Part 1: Dynamics of sand, wind and barchans. *Eur. Phys. J. B*, 28:321–339, 2002.

B. Andreotti, A. Fourrière, F. Ould-Kaddour, A. B. Murray, and P. Claudin. Giant aeolian dune size determined by the averaged depth of the atmospheric boundary layer. *Nature*, 457:1120–23, 2009.

B. Andreotti, P. Claudin, O. Devauchell, O. Durán, and A. Fourrière. Bedforms in a turbulent stream: ripples, chevrons and antidunes. *J. Fluid Mech.*, 690:94–128, 2012.

G. M. Ashley. Classification of large-scale subaqueous bedforms: A new look at an old problem. *J. Sediment. Petrol.*, 60:160–172, 1990.

R. A. Bagnold. *The physics of blown sand and desert dunes.* Methuen & Co., first edition, 1941.

P. L. Barnard, D. M. Haynes, D. M. Rubin, and R. G. Kvitek. Giant Sand Waves at the Mouth of San Francisco Bay. *Eos*, 87, 2006.

S. E. Belcher and J. C. R. Hunt. Turbulent flow over hills and waves. *Ann. Rev. Fluid Mech.*, 30:507–538, 1998.

T. B. Benjamin. Shearing flow over a wavy boundary. *J. Fluid Mech.*, 6:161–205, 1958.

J. Boussinesq. Essai sur la théorie des eaux courantes. *Mémoires présentés par divers savants à l'Académie des Sciences*, 23:1–680, 1887.

J. Buckles, T. J. Hanratty, and R. J. Adrian. Turbulent flow over large-amplitude wavy surfaces. *J. Fluid Mech.*, 140:27–44, 1984.

E. A. Caponi, B. Fornberg, D. D. Knight, J. W. McLean, P. G. Saffman, and H. C. Yeun. Calculations of laminar viscous flow over a moving wavy surface. *J. Fluid Mech.*, 124: 247–262, 1982.

F. Charru. Selection of the ripple length on a granular bed sheared by a liquid flow. *Phys. Fluids.*, 18, 2006.

F. Charru and E. M. Franklin. Subaqueous barchan dunes in turbulent shear flow. Part 2. Fluid flow. *J. Fluid Mech.*, 694:131–154, 2012.

F. Charru and E. J. Hinch. 'Phase diagram' of interfacial instabilities in a two-layer Couette flow and mechanism of the long-wave instability. *J. Fluid Mech.*, 414:195–223, 2000.

F. Charru and E. J. Hinch. Ripple formation on a particle bed sheared by a viscous liquid. Part 1. Steady flow. *J. Fluid Mech.*, 550:111–121, 2006.

F. Charru and H. Mouilleron-Arnould. Instability of a bed of particles sheared by a viscous flow. *J. Fluid Mech.*, 452:303–323, 2002.

F. Charru, H. Mouilleron, and O. Eiff. Erosion and deposition of particles on a bed sheared by a viscous flow. *J. Fluid Mech.*, 519:55–80, 2004.

F. Charru, B. Andreotti, and P. Claudin. Sand Ripples and Dunes. *Annu. Rev. Fluid. Mech.*, 45:469–493, 2013.

P. Claudin, F. Charru, and B. Andreotti. Transport relaxation time and length scales in turbulent suspensions. *J. Fluid Mech.*, 671:491–506, 2011.

S. Corrsin. Turbulent flow. *Am. Sci.*, 49:300–325, 1961.

P. A. Davidson. *Turbulence: An Introduction for Scientists and Engineers*. Oxford University Press, first edition, 2004.

O. Durán, V. Schẅammle, P. G. Lind, and H. J. Herrmann. Size distribution and structure of Barchan dune fields. *Nonlin. Processes Geophys.*, 18:455–467, 2011.

J. J. Finnigan, M. R. Raupach, E. F. Bradley, and G. K. Aldis. A wind-tunnel study of turbulent flow over a two-dimensional ridge. *Bound.-Layer Meteor.*, 50:277–317, 1990.

A. Fourrière, P. Claudin, and B. Andreotti. Bedforms in a turbulent stream: formation of ripples by primary instability and of dunes by non-linear pattern coarsening. *J. Fluid Mech.*, 649:287–328, 2010.

E. M. Franklin. Formation of sand ripples under a turbulent liquid flow. *Appl. Math. Model.*, 39:7390–7400, 2015.

E. M. Franklin and F. Charru. Subaqueous barchan dunes in turbulent shear flow. Part 1. Dune motion. *J. Fluid Mech.*, 675:199–222, 2011.

K. A. Frederick and T. J. Hanratty. Velocity measurements for a turbulent nonseparated flow over solid waves. *Exp. Fluids*, 6:477–486, 1988.

X. Gao, C. Narteau, and O. Rozier. Development and steady states of transverse dunes: A numerical analysis of dune pattern coarsening and giant dunes. *J. Geophys. Res. Earth Surf.*, 120:2200–2219, 2015.

D. S. Henn and R. I. Sykes. Large-eddy simulation of flow over wavy surfaces. *J. Fluid Mech.*, 383:75–112, 1999.

J. C. R. Hunt, S. Leibovich, and K. J. Richards. Turbulent shear flows over low hills. *Q. J. R. Meteorol. Soc.*, 114:1435–1470, 1988.

P. S. Jackson and J. C. R. Hunt. Turbulent wind flow over a low hill. *Quart. J. R. Met. Soc.*, 101:929–955, 1975.

P. Y. Julien. *Erosion and sedimentation*. Cambridge University Press, first edition, 1995.

J. W. Kamphuis. Determination of sand roughness for fixed beds. *J. Hydraul. Res.*, 12: 193–207, 1974.

J. Kim, P. Moin, and R. Moser. Turbulence statistics in fully developed channel flow at low reynolds number. *J. Fluid Mech.*, 177:133–166, 1987.

K. Kroy, G. Sauermann, and H. J. Herrmann. Minimal model for aeolian sand dunes. *Phys. Rev. E*, 66, 2002.

J. D. Kuzan, T. J. Hanratty, and R. J. Adrian. Turbulent flows with incipient separation over solid waves. *Exp. Fluids*, 7:88–98, 1989.

N. Lancaster. Controls of eolian dune size and spacing. *Geology*, 16:972–975, 1988.

V. Langlois and A. Valance. Initiation and evolution of current ripples on a flat sand bed under turbulent water flow. *Eur. Phys. J. E.*, 22:201–208, 2007.

D. Leighton and A. Acrivos. Viscous resuspension. *Chem. Eng. Sci.*, 41:1377–1384, 1986.

D. Leighton and A. Acrivos. The shear-induced migration of particles in concentrated suspensions. *J. Fluid Mech.*, 181:415–439, 1987.

H. Mouilleron, F. Charru, and O. Eiff. Inside the moving layer of a sheared granular bed. *J. Fluid Mech.*, 628:229–239, 2009.

P. R. Owen. Saltation of uniform grains in air. *J. Fluid. Mech.*, 20:225–242, 1964.

S. B. Pope. *Turbulent flows*. Cambridge University Press, first edition, 2000.

L. Prandtl. Bericht ber Untersuchungen zur ausgebildeten Turbulenz. *Z. Angew. Math. Mech.*, 5:136–139, 1925.

K. J. Richards and P. A. Taylor. A numerical model of flow over sand waves in water of finite depth. *Geophys. J. R. astr. Soc.*, 65:103–128, 1981.

R. L. Simpson, Y. Chew, and B. G. Shivaprasad. The structure of a separating turbulent boundary layer. Part 1. Mean flow and Reynolds stresses. *J. Fluid Mech.*, 113:23–51, 1981.

R. I. Sykes. An asymptotic theory of incompressible turbulent boundary-layer flow over a small hump. *J. Fluid Mech.*, 101:647–670, 1980.

T. von Kármán. Mechanische ähnlichkeit und Turbulenz. *Proc. Third Int. Congr. Applied Mechanics*, pages 85–105, 1930.

T. Wei and W. W. Willmarth. Reynolds-number effects on the structure of a turbulent channel flow. *J. Fluid Mech.*, 204:57–95, 1989.

A. Wierschem, C. Groh, I. Rehberg, N. Aksel, and C. A. Kruelle. Ripple formation in weakly turbulent flow. *Eur. Phys. J. E*, 25:213–221, 2008.

W. Yue, C. Lin, and V. C. Patel. Large-Eddy Simulation of Turbulent Flow over a Fixed Two-Dimensional Dune. *J. Hydraul. Eng.*, 132:643–651, 2006.

D. P. Zilker and T. J. Hanratty. Influence of the amplitude of a solid wavy wall on a turbulent flow. Part 2. Separated flows. *J. Fluid Mech.*, 90:257–271, 1979.

D. P. Zilker, G. W. Cook, and T. J. Hanratty. Influence of the amplitude of a solid wavy wall on a turbulent flow. Part 1. Non-separated flows. *J. Fluid Mech.*, 82:29–51, 1977.